Article

Journal of the Brazilian Chemical Society

https://dx.doi.org/10.21577/0103-5053.20240120

J. Braz. Chem. Soc. **2024**, *35*, 12, e-20240120, 1-9
©2024 Sociedade Brasileira de Química

Simple and Fast Preparation of Transparent Conductive Films of Silver Nanowires Obtained by a Salt Assisted Polyol Method

Barbara P. G. Silva,[a] Willian C. da Silva,[a] Stefany R. Saraiva[a] and Larissa Otubo[*,a]

[a]*Instituto de Pesquisas Energéticas e Nucleares (IPEN/CNEN), Av. Prof. Lineu Prestes, 2242, Cidade Universitária, 05508-000 São Paulo-SP, Brazil*

Silver nanowires thin films have gained attention due to their excellent optical and electrical properties, being a potential material to be applied in optoelectronic devices as transparent conductive films, deposited on a substrate in a such way that forms a percolated network. We report the synthesis of silver nanowires with average length of 9.5 ± 0.4 μm and diameter of 75 ± 3 nm by a modified polyol method and fabrication of transparent and conductive thin films using a simple and low-cost technique as drop-casting. Additionally, we examined the influence of the drop-casting method in function of number of deposition cycles on the optical and electrical properties of the films through optical absorption and electrical resistance measurements using the two-point methodology. Increasing the number of silver nanowire deposition layers, the optical transmittance decreased from 97 (for one layer) to 60% (for five layers), and electrical resistance decreased from 940 ± 0.35 Ω for the 2-layer film to 32 ± 0.02 Ω, for the 5-layer film. Due to the electrical conductivity range of the produced silver nanowires films, we suggested their application in low-voltage circuits.

Keywords: silver nanowires, polyol method, transparent conductive films, drop-casting

Introduction

Transparent conductive films (TCFs) have been extensively studied in recent years due to their applications in electronic devices such as light emitting diodes (LEDs), solar cells, and displays. Nowadays, indium tin oxide (ITO) stands as the predominant material in electronic device manufacturing, due to its high transmittance (> 80% at $\lambda = 550$ nm) and low electrical resistivity (ca. 10-4 Ω cm).[1,2] However, the scarcity and costliness of indium, coupled with its mechanical rigidity, constrain its application in flexible materials.

Aiming to seek alternatives to ITO, different materials have been studied to be applied in the production of TCFs as conductive polymers,[3,4] carbon nanotubes,[5,6] graphene,[7-9] and metallic nanowires.[10-13] Among these, metallic nanowires have attracted attention due to their electrical, mechanical, thermal, and optical properties. This type of material can be synthesized through several routes and one of the most commonly employed is the polyol method.[14] Researchers have extensively examined and modified this method, particularly by incorporating mediator salts (as Cl^- and Br^- ions), that exert a crucial role in the nanowire formation process, reducing the reaction kinetics,[15-17] and guiding the wire morphology growth[18-20] enabling the production of longer and thinner wires.[21] The Br^- and Cl^- ions complex with Ag^+ ions and form AgBr and AgCl salts respectively, thereat, the concentration of free Ag^+ ions are reduced in the reaction solution resulting in stable multiple twinned particles (MPTs).[22] The method involves the reduction of a metallic precursor compound by a polyol, and the stabilization and growth of the structure are facilitated by a capping agent. Polyol method is widely used for its simplicity and the use of low temperatures, employing silver as the most utilized material in the synthesis of metallic nanowires,[23-25] primarily due to its electrical and optical properties.

Studies[26-28] demonstrate that experimental parameters such as reaction time, temperature, and reagent concentration, for example, impact on the crystallinity, morphology, and size of the obtained material. In the context of elaborating TCFs, the control of these parameters is crucial. For instance, silver nanowires (AgNWs) with well-defined morphology, good crystallinity, and high aspect ratio can facilitate the formation of percolated networks with enhanced optical and electrical properties.

*e-mail: larissa.otubo@ipen.br
Editor handled this article: Aldo José Gorgatti Zarbin (Guest)

This is an open-access article distributed under the terms of the Creative Commons Attribution License.

In addition to morphological and structural parameters, the technique employed for depositing nanowires onto a substrate can influence the properties of the resulting films. In this context, methods such as spray-coating, spin-coating, and drop-casting have been explored.[29,30] Among these, the drop-casting technique stands out for being an easily applicable method without significant loss of the filmogenic suspension. However, the uniformity of the resulting film is associated with the liquid dynamics during the solvent drying process, fundamentally dependent on the surface tension of the solvent and the hydrophilicity of the substrate. These characteristics make the process complex, motivating the investigation of the influence of this method on 1D-structured TCFs, such as silver nanowires.[31]

In this study, we report the synthesis and characterization of silver nanowires and their application in the development of transparent films on glass slide, investigating the influence of the properties of the nanowires and the drop-casting technique on the optical and electrical characteristics of the resulting films. X-ray diffractometry (XRD), transmission electron microscopy (TEM), scanning electron microscopy (SEM), atomic force microscopy (AFM), UV-Vis spectroscopy and electrical resistance were employed to characterize the synthesized AgNWs and AgNWs films.

Experimental

Chemicals

The chemicals used were: silver nitrite ($AgNO_3$, Sigma-Aldrich, Gillingham, United Kingdom), polyvinylpyrrolidone 1300K (PVP, Mw ca. 1,300,000 g mol^{-1}, Sigma-Aldrich, Darmstadt, Germany), sodium bromide (NaBr, Synth, Diadema, Brazil), sodium chloride (NaCl, Synth, Diadema, Brasil), ethylene glycol (EG, Synth, Diadema, Brazil), ethanol (Alphatec, São Bernardo do Campo, Brasil), acetone (Alphatec, São Bernardo do Campo, Brazil), ammonium hydroxide (NH_4OH, Alphatec, São Bernardo do Campo, Brazil), hydrogen peroxide (30%, H_2O_2, Alphatec, São Bernardo do Campo, Brazil). All chemical products are analytical grade and were used without further purification.

Preparation of silver nanowires

The silver nanowires were synthesized by polyol method assisted by salt. In a typical synthesis, 5.2 mmol of PVP was dissolved in 20 mL of EG, followed by addition of 3.5 mmol of $AgNO_3$, 1.5 mL of 0.005 mol L^{-1} NaBr solution and 0.5 mL of 0.01 mol L^{-1} NaCl solution. Then, the round-bottom flask with all the reactants was placed in a preheated oil bath (at 175 °C) for 20 min under reflux and magnetic stirring. After the end of the reaction, the mixture was washed with ethanol and centrifuged several times (8,000 rpm for 5 min), until the supernatant became clear. The obtained material was redispersed in ethanol for further analysis and characterization.

Preparation of silver nanowires transparent conductive films

The films were prepared using glass slide as substrates (1 × 1 cm). Before use, the glass slides were cleaned in an ultrasonic bath subsequently using acetone, water and ethanol, respectively for 15 min each, at room temperature. After the cleaning process, a surface treatment was performed on these substrates to increase the surface polarity. This was achieved by immersing them in a solution of H_2O:NH_4OH:H_2O_2 (5:1:1 v:v:v) for 30 min at 80 °C and then drying at room temperature.

Before applying the AgNWs to the films, a purification of the synthesized material was carried out to select the thinner and longest nanowires. For this purpose, the AgNW-containing suspension was centrifuged with ethanol (at 3,000 rpm for 5 min), and the supernatant, containing the longer and thinner wires, was collected and used for the film deposition on the substrate.

Then, an amount of 50 µL of the purified AgNWs ethanolic suspension was drop-casted on the substrates using a pipette, and dried in an oven under atmospheric conditions at 120 °C for 15 min. Different densities of AgNWs films were obtained by varying the number of layers, from 1 to 5, following the drop-cast deposition and solvent evaporation (at 120 °C for 15 min) in each cycle.

Characterization

The morphology of silver nanowires was observed by scanning electron microscopy (SEM), performed in a TM-3000 microscope (Hitachi, Toronto, Canada), operating at an acceleration voltage of 15 kV and by atomic force microscopy (AFM), using a Multimode 8 microscope (Bruker, Santa Barbara, USA), operating in tapping mode (probe RTESPA; resonance frequency = 300 kHz, Bruker). For that, the sample suspension was dropped on a glass substrate and dried at 80 °C. The optical absorption spectra of the ethanolic AgNW suspension were obtained in a UV-Vis spectrophotometer Cary 5000 (Agilent, Santa Clara, USA) suspension, using a quartz cuvette. The morphological and structural characterization of the nanowires was analyzed by transmission electron microscopy (TEM), using a JEM-2100 microscope (JEOL, Peabody, USA), operating at an acceleration voltage of 200 kV. The suspension of AgNWs was dropped on a 400 mesh copper grid coated with a collodion/

carbon film. For structural analysis, X-ray diffraction (XRD) was performed in a SmartLab SE (Rigaku, Akishima, Japan) using CuK (λ = 1.54 Å) radiation as incident beam.

The AgNWs films with different number of layers were characterized by scanning electron microscopy and optical transmittance measurements, using the same equipment employed for the optical and morphological characterizations of the nanowires.

To investigate the electrical properties of the films, electrical resistance measurements were conducted in three different configurations: time-dependent electrical resistance measurements, determination of the current-voltage characteristic (I × V) curves of the films, and measurement of resistance in alternating voltage cycles (0 to 5 V), all at room temperature.[32,33]

For these measurements, two linearly spaced contacts were made at the center of each sample. These contacts were established using silver ink, serving the purpose of connecting the surface of the films to copper wires connected to two Kelvin probes. The spacing between the contacts was 50 mm (see Figure S1 presented in the Supplementary Information (SI) section).

For time-dependent electrical resistance measurements, an 8808A digital multimeter (Fluke, Everett, USA) was used, and measurements were conducted over 5 min, with the resistance value acquired every 10 s. The current-voltage (I × V) curves of the films were obtained in the range of 1 to 5 V. For these measurements, a source with variable voltage output was used, with the Fluke 8808A multimeter configured in ammeter mode and the ET-2042D multimeter (Minipa, São Paulo, Brazil) in voltmeter mode (Figure S2 in SI section).

As measurements of electrical resistance in voltage cycles were conducted to assess the stability of the electrical resistance of the films under voltage variations. For these measurements, the films were connected to a microcontroller (Arduino UNO) with a C++ program responsible for voltage variations on the logic port connected to the film (Figure S3 in SI section). The voltage variations on the logic port were programmed to oscillate from 0 to 5 V every second, and a resistance measurement was taken with each variation.[32,34]

Results and Discussion

AgNWs formation mechanism

The mechanism for the formation of silver nanowires involves the reduction of silver ions, the formation and nucleation of seeds, and the ordered growth of crystals, which is limited by the reduction rate.[28,35]

In the polyol method, ethylene glycol is heated, leading to the formation of acetaldehyde (equation 1), which acts as the reducing agent for silver ions (equation 2).[19,36]

$$2HOCH_2CH_2OH \rightarrow 2CH_3CHO + 2H_2O \quad (1)$$

$$2Ag^+ + 2CH_3CHO \rightarrow 2Ag + CH_3CO{-}OCCH_3 + 2H^+ \quad (2)$$

The growth of the structures can be directed by adding a capping agent, such as PVP or some halide ions which adsorbs preferentially onto the {100} face of silver, acting as a passivator during the silver ion reduction and favoring the growth in the [111] direction.[37,38] Thereby, the steric effect of the PVP long chains prevents silver particles from aggregating and coalescing, playing a crucial role in the formation and stabilization of these nanostructured materials.[39]

In this study, silver nitrate was used as the metal precursor, PVP, NaBr and NaCl as growth-directing agents. NaBr and mostly NaCl have also an important role on the growth kinetics control of AgNWs through the formation of AgCl/AgBr which have a small solubility constant. Besides acting as crystal seeds, with the increase of reaction temperature, Ag^+ ions are slowly released through AgCl and AgBr dissociation and reduced to Ag^0 by EG, favoring the longitudinal growth of the nanowire (Figure 1).[21]

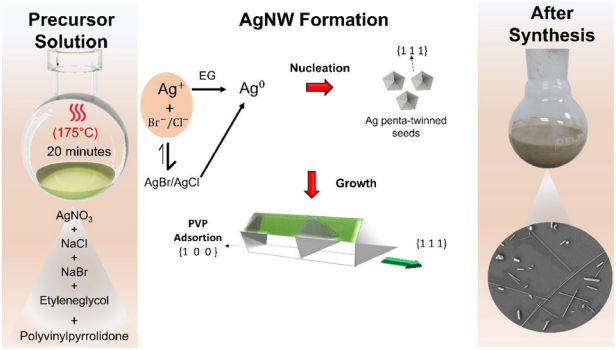

Figure 1. Formation of silver nanowires using polyol method.

Silver nanowires were successfully synthesized, resulting in a mixture consisting of a high amount of long and thin nanowires, along with other morphologies such as particles and rods (Figure 2a). For the film depositions, the nanowire suspension was purified in order to remove those denser nanoparticles, prevailing the longer and thinner nanowires. Before purification, the longest measured nanowires had a length of approximately 30 μm, with an average size (L_a) of 9.5 ± 0.4 μm and a diameter (D_a) of 75 ± 3 nm (Figures 2b and 2c).

The AgNWs have a smooth and regular surface, as can be seen in the AFM topography image (Figure 3a). Additionally, the wires exhibit rounded shapes with varying heights (Figure 3b),

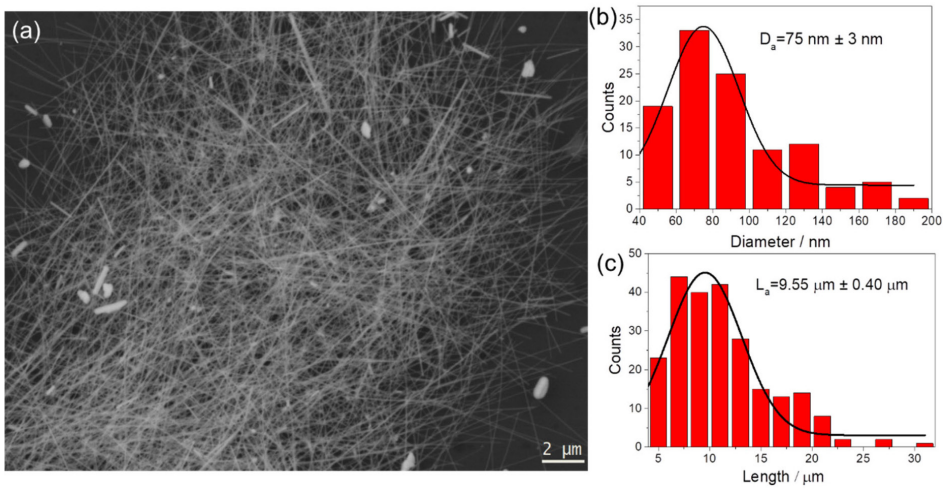

Figure 2. SEM images of AgNWs synthesized by polyol method (a) and statistical distribution of diameter (b) and length (c).

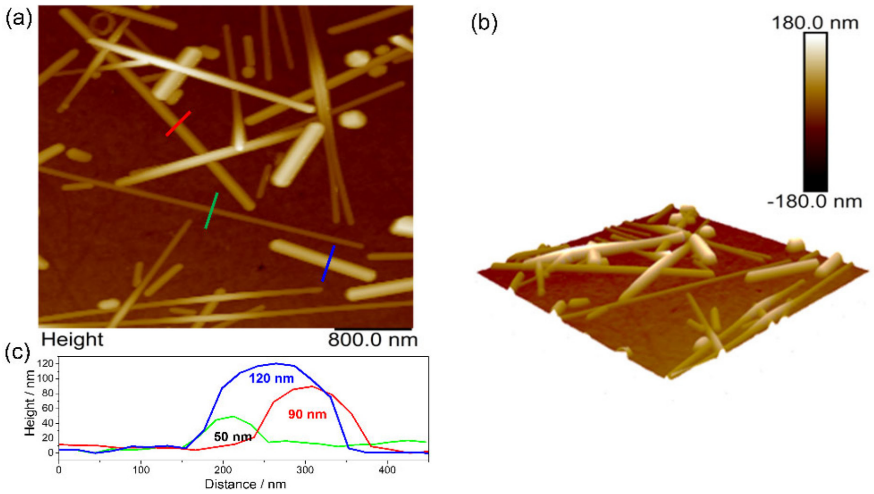

Figure 3. AFM images of AgNWs represented in (a) height, (b) 3D and (c) graphical representation of cross section of the lines drawn in image (a).

as evidenced by cross-section analysis (Figure 3c), consistent with measurements taken from SEM images.

The crystalline features of the AgNWs were analyzed by XRD. The XRD pattern for the silver nanowires was refined using the Rietveld method in refinement cycles (Figure 4). The results are consistent with standard peaks of the face-centered cubic phase (Ag-fcc), as indicated by the crystallographic pattern (mp-124). The crystallite size obtained through the Scherrer equation is 20 nm. The results suggest a preferential orientation in the (111) plane, in accordance with the proposed formation mechanism and morphological characteristic of the samples observed by SEM and AFM.[38,40]

The TEM results show the formation of AgNWs with an organic layer of approximately 3 nm covering the wire, which can be attributed to PVP adsorbed onto the surface during the growth phase (Figure 5a and inset). The capping agent acts as a stabilizer, preventing the agglomeration and oxidation of the nanowires. On the other hand, the

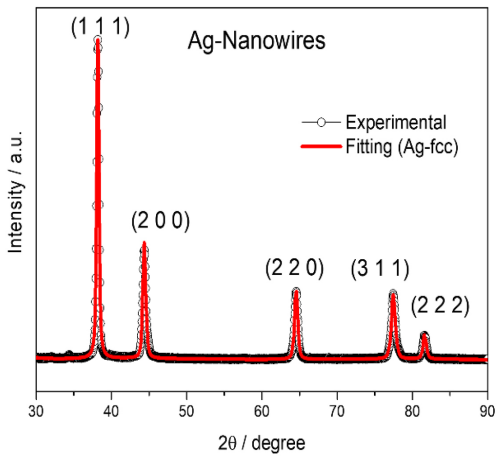

Figure 4. XRD diffractogram of silver nanowires.

thickness of the layer can influence the electrical properties of percolating networks of nanowires.[41] For the produced AgNW films, this effect might have been diminished by the drying temperature (120 °C) used after each deposition

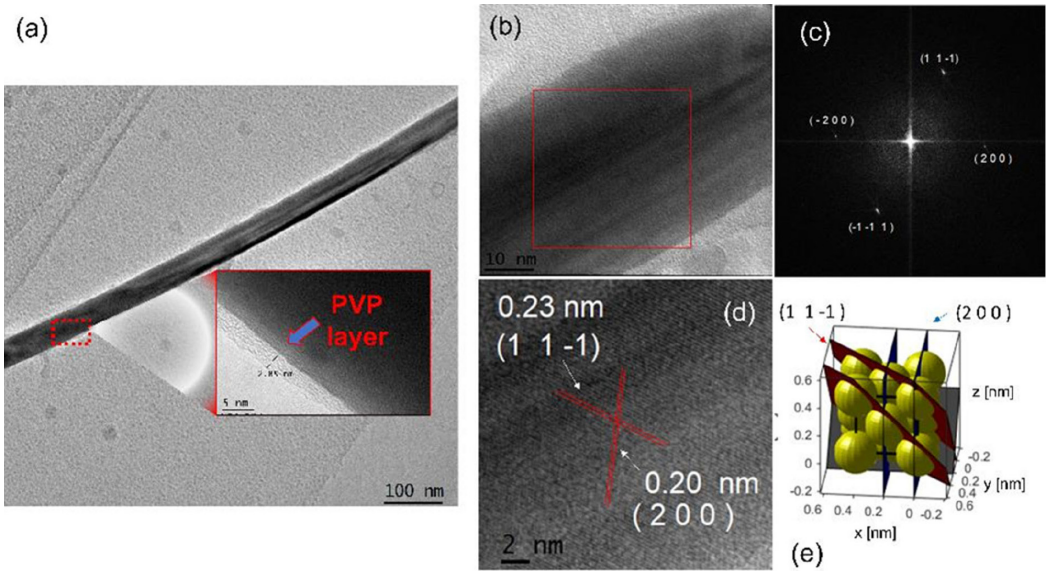

Figure 5. TEM images of AgNW represented in (a) longitudinal section with a PVP layer, (b) longitudinal section of the nanowire at higher magnification, (c) FFT, (d) Ag-fcc planes indexed along the [001] zone axis and (e) theoretical representation of the presented planes.

cycle. Figures 5b and 5d show images of the longitudinal section of an AgNW in higher magnifications. The fast Fourier transform (FFT) obtained for this region (Figure 5c) reveals crystalline planes with interplanar distances of 0.23 and 0.20 nm, consistent with the (11–1) and (200) planes of Ag-fcc, respectively, depicted in Figure 5d along the [011] zone axis, as indexed from the crystallographic pattern (mp-124). Figure 5e illustrates the theoretical crystalline structure representation of these planes.[40,42]

In order to analyze and characterize the AgNWs optical properties, UV-Vis spectroscopy was employed. It is well known that silver nanostructures have the different shapes and morphologies associated to surface plasmon resonance (SPR).[43] A typical AgNWs spectra can be seen on Figure 6, where two characteristic peaks can be observed at 353 and 385 nm and they can be attributed to the transversal mode of silver nanowires.[44,45]

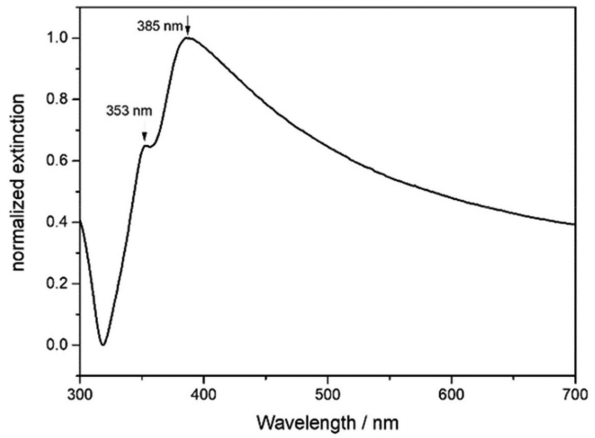

Figure 6. Normalized UV-Vis extinction spectra of silver nanowires dispersed in ethanol.

From a dispersion of the purified material in absolute ethanol, films were constructed on glass slides using drop-casting, which is a simple, easy, and fast deposition method.[43] These films were examined using SEM, showing the distribution of the deposited material (Figure 7). Increasing the number of layers resulted in a higher material density, as expected, however in less homogeneous films, which can be attributed to the deposition technique used.[44]

The optical transmittance is an important property for TCF and in the case of AgNW films can be optimized by changing the network density, the distribution of AgNWs on the substrate by changing the deposition method and also by tunning the AgNW morphology, by decreasing the diameter.[10,24,46,47] In order to evaluate optical properties of the AgNWs films, UV-Vis spectroscopy was used in the transmittance mode using pristine glass as the baseline. As expected, increasing the amount of the deposited material on the glass substrate through the deposition cycles, a gradual decreasing in the light transmittance could be observed, ranging from 97% (1 layer) to approximately 60% (5 layers) at 550 nm (inset of Figure 8a). Also, it is possible to verify that the transmittance of AgNW films is fairly stable across almost the entire visible range (Figure 8a). Except for the 5-layer AgNW film, regarding the optical transmittance, the materials have potential to be used as TCFs, as in comparison with ITO and carbon nanotubes films.[2] Figure 8b shows pictures of the AgNW films from 1 to 5 layers, where the transparency of the materials can be observed even after 5 cycles of deposition, illustrating the transmittance measured by UV-Vis spectroscopy. Besides transmittance, optical haze is an important parameter to be studied in AgNW films because of its high dependence with

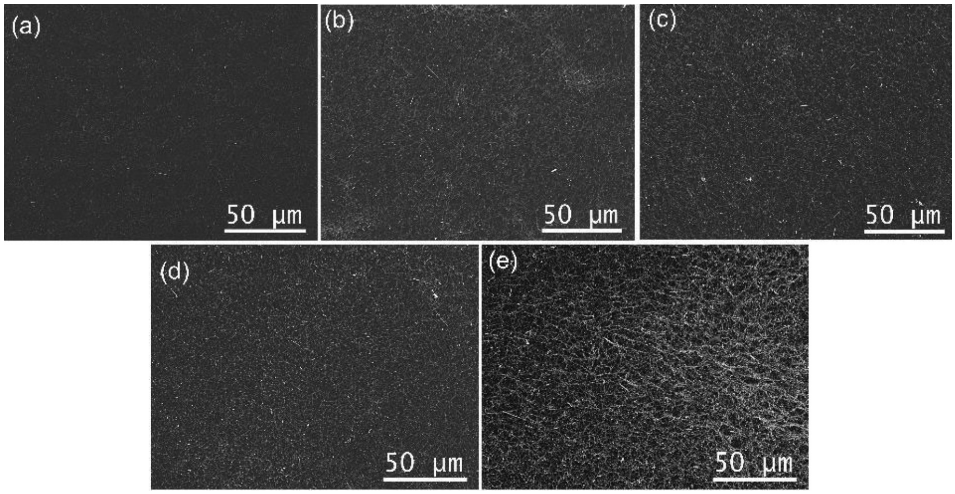

Figure 7. SEM images of AgNWs films on glass substrate from 1 to 5 layers, (a) to (e), respectively.

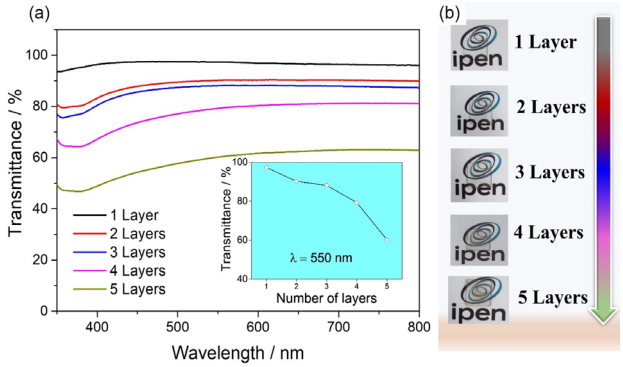

Figure 8. Transmittance spectra (a) and pictures (b) of AgNWs films on glass substrates from 1 to 5 layers. The inset in (a) indicates the transmittance of the films at 550 nm in function of the number of layers.

the geometry of the nanostructure, specially the nanowire diameter.[48-50]

Electrical resistance measurements

The electrical resistance measurements using the two-probe method revealed variations in the electrical properties of the films in function of the number of layers. The sample with a single layer showed no measurable resistance values within the reading range of the equipment. This suggests the absence of electrical percolation among the nanowires deposited in the film. The average resistances obtained for the other samples were 940 ± 0.35, 2565 ± 1.40, 422 ± 0.20, and 32 ± 0.02 Ω, for films with 2, 3, 4, and 5 layers, respectively (Figure 9). The results suggest a decrease in electrical resistance with increasing number of layers for samples with 2, 4, and 5 layers. On the other hand, the high resistance value for the one-layer sample and the discrepancy of the resistance value obtained for the 3-layer film, may be related to the non-uniform distribution of the nanowires during drop-casting deposition and film formation. According to the literature,[51,52] the macroscopic electrical conductivity of nanowire films is mostly dependent on the formation of a percolated network, which is mainly influenced by the network density and physical characteristics of the nanowires (as diameter, length and joint resistance). The percolating network density will modify the electrical and optical properties of the nanowire films, that could determine the applicability of these materials.[51,53] In this sense, comparing the optical transmittance values and the electrical resistance in function of the number of layers deposited elucidates that, although there is a decrease in the optical transmittance with the increase of the number of layers (Figure 8) due to a bigger amount of nanowires on the film surface, their random distribution on the surface may cause the non-proportional relation of the electrical resistance and the increase of the number of nanowire layers, as expected.[51,54] Therefore, many theoretical and experimental studies[54-56] have been

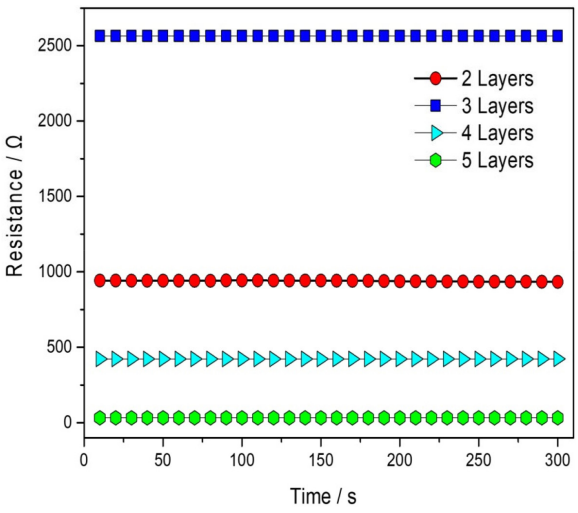

Figure 9. Electrical resistance measurements over time for samples with different numbers of layers.

made to verify the AgNWs network formation through different approaches like spin-coating, spray deposition and drop-casting. The nanowire network formation by those methodologies is random, as predicted by theoretical models and experimental observations.[31,52] Furthermore, for drop-casting, that was the chosen technique to produce the studied AgNWs films here, there are effects caused by interaction with the substrate, related to the deposition and solvent evaporation (as the coffee-ring formation), can also promote a non-uniform electrical resistance behavior, which justifies the discrepancies of the resistance values in function of the number of layers.[31,57,58]

The determination of the characteristic curve of the films in the voltage range of 1 to 5 V suggests ohmic behavior for the films with 2, 3, 4, and 5 layers in this voltage range, as indicated by the linear fit presented in Figure 10. The electrical resistance results obtained by adjusting the values of current and voltage show good agreement with the values measured over time (see Tables S1 to S4 in SI section).

The resistance measurements in voltage cycles suggest that the films maintain resistance values despite continuous voltage variations (Figure 11a). The low electrical resistance observed for the AgNWs films and their performance facilitate the application of these films in low-voltage circuits.[59] Figure 11b shows the application of the 5-layer film (32 Ω) as a resistive element responsible for protecting one LED in a 2 V circuit powered by Arduino. However, although this considerably good electronic performance, for optoelectronic applications, the optical and the electrical properties must be both considered. Therefore, for the produced films by this methodology, the 4-layer film plays the best optical transmittance and electrical resistance relationship.

Conclusions

Silver nanowires stabilized with PVP were synthesized using a salt assisted polyol method, producing wires with an average length of approximately 9.5 μm and diameter of 75 nm (aspect ratio = 133), with well-defined morphology and crystallinity. Transparent films on glass were then constructed from the previously synthesized material using the drop-casting technique varying numbers of layers. The results demonstrated significant changes in the optical absorption of the films based on the number of layers. Although the electrical properties of AgNWs films are often discussed in the literature in terms of sheet resistance (Ohms *per* square), in this study, we opted for the use of resistance considering two points of the sample, enabling a quick and practical approach for film application. The electrical resistance measurements showed significant reductions in electrical resistance based on the increasing number of layers, however, these variations are not uniform due to the non-uniformity associated with the deposition technique.

The current-voltage curves obtained, associated with electrical resistance measurements in voltage cycles

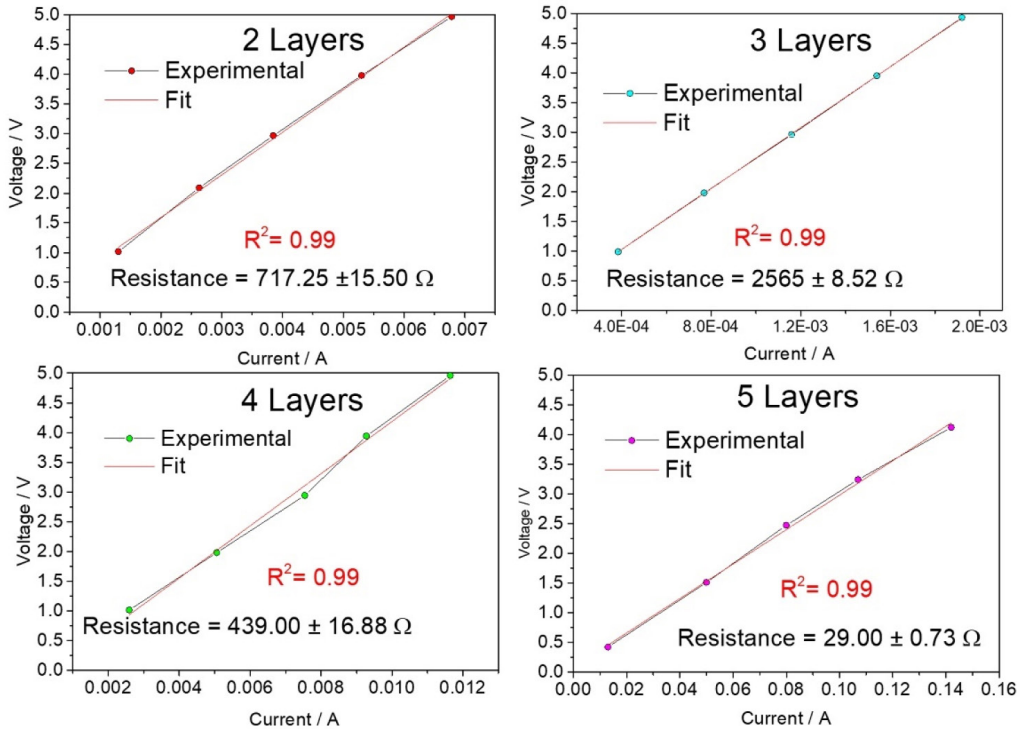

Figure 10. Current-voltage curve for the samples with 2 to 5 layers.

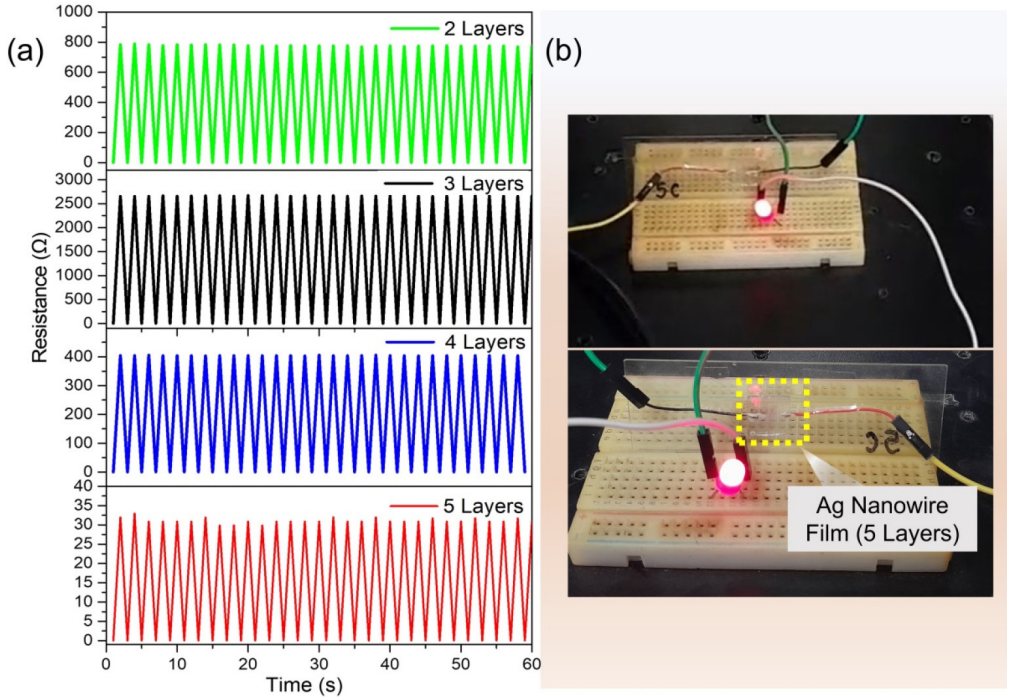

Figure 11. Measurements and application. (a) Resistance measurements in voltage cycles and (b) application using Arduino.

ranging from 0 to 5 V, suggest the possibility of applying these AgNWs films in low-voltage circuits, powered by devices like Arduino, for example. Additionally, the use of flexible substrates and the incorporation of semiconductor nanomaterials could be alternatives for enhancements and diverse applications of these systems in sensors.

Supplementary Information

Supplementary data (representative schemes of the experimental setup used for electrical measurements, data tables, equations, C++ code for obtaining electrical resistance in voltage cycles) are available free of charge at http://jbcs.sbq.org.br, as PDF file.

Acknowledgments

The authors thank IPEN/CNEN (2020.06.IPEN.22), CNPq (143546/2023-6 and 140981/2023) for financial support. We thank the support given by the Center for Lasers and Applications' Multiuser Facility at IPEN/CNEN-SP. Additionally, we thank the Microscopy and Microanalysis Laboratory (LMM/IPEN/CNEN-SP) for the characterizations.

References

1. Farhan, M. S.; Zalnezhad, E.; Bushroa, A. R.; Sarhan, A. A. D.; *Int. J. Precis. Eng. Manuf.* **2013**, *14*, 1465. [Crossref]
2. Ellmer, K.; *Nat. Photonics* **2012**, *6*, 809. [Crossref]
3. Zou, J.; Yip, H. L.; Hau, S. K.; Jen, A. K. Y.; *Appl. Phys. Lett.* **2010**, *96*, 203301. [Crossref]
4. Na, S.; Kim, S.; Jo, J.; Kim, D.; *Adv. Mater.* **2008**, *20*, 4061. [Crossref]
5. Zhang, G.; Duan, Z.; Wang, Q.; Li, L.; Yao, W.; Liu, C.; *Appl. Surf. Sci.* **2018**, *427*, 628. [Crossref]
6. Hu, L.; Hecht, D. S.; Grüner, G.; *Appl. Phys. Lett.* **2009**, *94*, 081103. [Crossref]
7. Kymakis, E.; Savva, K.; Stylianakis, M. M.; Fotakis, C.; Stratakis, E.; *Adv. Funct. Mater.* **2013**, *23*, 2742. [Crossref]
8. Yamaguchi, H.; Eda, G.; Mattevi, C.; Kim, H.; Chhowalla, M.; *ACS Nano* **2010**, *4*, 524. [Crossref]
9. Bae, S.; Kim, H.; Lee, Y.; Xu, X.; Park, J. S.; Zheng, Y.; Balakrishnan, J.; Lei, T.; Ri Kim, H.; Song, Y. I.; Kim, Y. J.; Kim, K. S.; Özyilmaz, B.; Ahn, J. H.; Hong, B. H.; Iijima, S.; *Nat. Nanotechnol.* **2010**, *5*, 574. [Crossref]
10. Bardet, L.; Papanastasiou, D. T.; Crivello, C.; Akbari, M.; Resende, J.; Sekkat, A.; Sanchez-Velasquez, C.; Rapenne, L.; Jiménez, C.; Muñoz-Rojas, D.; Denneulin, A.; Bellet, D.; *Nanomaterials* **2021**, *11*, 2785. [Crossref]
11. Gu, J.; Wang, X.; Chen, H.; Yang, S.; Feng, H.; Ma, X.; Ji, H.; Wei, J.; Li, M.; *Nanotechnol.* **2018**, *29*, 265703. [Crossref]
12. Cai, L.; Zhang, S.; Zhang, Y.; Li, J.; Miao, J.; Wang, Q.; Yu, Z.; Wang, C.; *Adv. Mater. Technol.* **2018**, *3*, 1700232. [Crossref]
13. Bob, B.; Machness, A.; Song, T. B.; Zhou, H.; Chung, C. H.; Yang, Y.; *Nano Res.* **2016**, *9*, 392. [Crossref]
14. Fievet, F.; Lagier, J.; Blin, B.; Beaudoin, B.; Figlarz, M.; *Solid State Ionics* **1989**, *32-33*, 198. [Crossref]

15. Parente, M.; van Helvert, M.; Hamans, R. F.; Verbroekken, R.; Sinha, R.; Bieberle-Hütter, A.; Baldi, A.; *Nano Lett.* **2020**, *20*, 5759. [Crossref]
16. Coskun, S.; Aksoy, B.; Unalan, H. E.; *Cryst. Growth Des.* **2011**, *11*, 4963. [Crossref]
17. Nghia, N. V.; Truong, N. N. K.; Thong, N. M.; Hung, N. P.; *Int. J. Mater. Chem.* **2012**, *2*, 75. [Crossref]
18. Rui, Y.; Zhao, W.; Zhu, D.; Wang, H.; Song, G.; Swihart, M.; Wan, N.; Gu, D.; Tang, X.; Yang, Y.; Zhang, T.; *Nanomaterials* **2018**, *8*, 161. [Crossref]
19. Cao, L.; Huang, Q.; Cui, J.; Lin, H.; Li, W.; Lin, Z.; Zhang, P.; *Nanomaterials* **2020**, *10*, 1139. [Crossref]
20. da Silva, R. R.; Yang, M.; Choi, S. I.; Chi, M.; Luo, M.; Zhang, C.; Li, Z. Y.; Camargo, P. H. C.; Ribeiro, S. J. L.; Xia, Y.; *ACS Nano* **2016**, *10*, 7892. [Crossref]
21. Tang, C.; Sun, W.; Lu, J.; Yan, W.; *J. Colloid Interface Sci.* **2014**, *416*, 86. [Crossref]
22. Fahad, S.; Yu, H.; Wang, L.; ul-Abdin, Z.; Haroon, M.; Ullah, R. S.; Nazir, A.; Naveed, K. R.; Elshaarani, T.; Khan, A.; *J. Mater. Sci.* **2019**, *54*, 997. [Crossref]
23. Zhang, X.; Wu, J.; Liu, H.; Wang, J.; Zhao, X.; Xie, Z.; *Org. Electron.* **2017**, *50*, 255. [Crossref]
24. De, S.; Higgins, T. M.; Lyons, P. E.; Doherty, E. M.; Nirmalraj, P. N.; Blau, W. J.; Boland, J. J.; Coleman, J. N.; *ACS Nano* **2009**, *3*, 1767. [Crossref]
25. Hu, L.; Kim, H. S.; Lee, J. Y.; Peumans, P.; Cui, Y.; *ACS Nano* **2010**, *4*, 2955. [Crossref]
26. Wiley, B.; Sun, Y.; Xia, Y.; *Acc. Chem. Res.* **2007**, *40*, 1067. [Crossref]
27. Rycenga, M.; Cobley, C. M.; Zeng, J.; Li, W.; Moran, C. H.; Zhang, Q.; Qin, D.; Xia, Y.; *Chem. Rev.* **2011**, *111*, 3669. [Crossref]
28. Hemmati, S.; Harris, M. T.; Barkey, D. P.; *J. Nanomater.* **2020**, *2020*, 1. [Crossref]
29. Ha, H.; Amicucci, C.; Matteini, P.; Hwang, B.; *Colloid Interface Sci. Commun.* **2022**, *50*, 100663. [Crossref]
30. Lahane, T. K.; Agrawal, J.; Ando, Y.; Pandey, S. S.; Singh, V.; *Phys. Status Solidi* **2023**, *220*, 2300166. [Crossref]
31. Fox, D. W.; Schropp, A. A.; Joseph, T.; Azim, N.; Li Sip, Y. Y.; Zhai, L.; *ACS Appl. Nano Mater.* **2021**, *4*, 7628. [Crossref]
32. Gurarslan, A.; Özdemir, B.; Bayat, I. H.; Yelten, M. B.; Kurt, G. K.; *J. Eng. Fibers Fabr.* **2019**, *14*, 1. [Crossref]
33. Casanova-Chafer, J.; Garcia-Aboal, R.; Atienzar, P.; Feliz, M.; Llobet, E.; *ACS Appl. Mater. Interfaces* **2022**, *14*, 57122. [Crossref]
34. Mustafa, K. R.; Mustafa, R. M.; Ramadani, R. M.; *Asian J. Res. Comput. Sci.* **2023**, *16*, 211. [Crossref]
35. Murph, S. E. H.; Murphy, C. J.; Leach, A.; Gall, K.; *Cryst. Growth Des.* **2015**, *15*, 1968. [Crossref]
36. Chen, C.; Wang, L.; Jiang, G.; Yang, Q.; Wang, J.; Yu, H.; Chen, T.; Wang, C.; Chen, X.; *Nanotechnology* **2006**, *17*, 466. [Crossref]
37. Al-Saidi, W. A.; Feng, H.; Fichthorn, K. A.; *Nano Lett.* **2012**, *12*, 997. [Crossref]
38. Guo, Y.; Hu, Y.; Luo, X.; Lin, S.; Hu, J.; Liu, Y.; *Inorg. Chem. Commun.* **2021**, *128*, 108558. [Crossref]
39. Zhang, Z.; Zhao, B.; Hu, L.; *J. Solid State Chem.* **1996**, *121*, 105. [Crossref]
40. Zhang, S. B.; *Comput. Mater. Sci.* **2014**, *95*, 53. [Crossref]
41. Hwang, J.; Shim, Y.; Yoon, S. M.; Lee, S. H.; Park, S. H.; *RSC Adv.* **2016**, *6*, 30972. [Crossref]
42. Klinger, M.; *J. Appl. Crystallogr.* **2017**, *50*, 1226. [Crossref]
43. Sohn, H.; Park, C.; Oh, J. M.; Kang, S. W.; Kim, M. J.; *Materials* **2019**, *12*, 2526. [Crossref]
44. Gao, Y.; *J. Funct. Biomater.* **2018**, *9*, 16. [Crossref]
45. Sun, Y.; Gates, B.; Mayers, B.; Xia, Y.; *Nano Lett.* **2002**, *2*, 165. [Crossref]
46. Zhang, J.; Zhu, X.; Xu, J.; Xu, R.; Yang, H.; Kan, C.; *Molecules* **2022**, *27*, 8907. [Crossref]
47. Yang, J.; Zeng, W.; Li, Y.; Yi, Z.; Zhou, G.; *Micromachines* **2020**, *11*, 1027. [Crossref]
48. Preston, C.; Xu, Y.; Han, X.; Munday, J. N.; Hu, L.; *Nano Res.* **2013**, *6*, 461. [Crossref]
49. Menamparambath, M. M.; Yang, K.; Kim, H. H.; Bae, O. S.; Jeong, M. S.; Choi, J. Y.; Baik, S.; *Nanotechnology* **2016**, *27*, 465706. [Crossref]
50. Ye, S.; Rathmell, A. R.; Chen, Z.; Stewart, I. E.; Wiley, B. J.; *Adv. Mater.* **2014**, *26*, 6670. [Crossref]
51. Bellet, D.; Lagrange, M.; Sannicolo, T.; Aghazadehchors, S.; Nguyen, V.; Langley, D.; Muñoz-Rojas, D.; Jiménez, C.; Bréchet, Y.; Nguyen, N.; *Materials* **2017**, *10*, 570. [Crossref]
52. Diaz-Alvarez, A.; Higuchi, R.; Sanz-Leon, P.; Marcus, I.; Shingaya, Y.; Stieg, A. Z.; Gimzewski, J. K.; Kuncic, Z.; Nakayama, T.; *Sci. Rep.* **2019**, *9*, 14920. [Crossref]
53. Manning, H. G.; da Rocha, C. G.; Callaghan, C. O.; Ferreira, M. S.; Boland, J. J.; *Sci. Rep.* **2019**, *9*, 11550. [Crossref]
54. Gomes da Rocha, C.; Manning, H. G.; O'Callaghan, C.; Ritter, C.; Bellew, A. T.; Boland, J. J.; Ferreira, M. S.; *Nanoscale* **2015**, *7*, 13011. [Crossref]
55. Zhang, L.; Song, T.; Shi, L.; Wen, N.; Wu, Z.; Sun, C.; Jiang, D.; Guo, Z.; *J. Nanostruct. Chem.* **2021**, *11*, 323. [Crossref]
56. Shi, Y.; He, L.; Deng, Q.; Liu, Q.; Li, L.; Wang, W.; Xin, Z.; Liu, R.; *Micromachines* **2019**, *10*, 330. [Crossref]
57. Liu, B. T.; Li, C. D.; *J. Taiwan Inst. Chem. Eng.* **2019**, *95*, 569. [Crossref]
58. Chavalitkul, J.; Margeat, O.; Ackermann, J.; Dubas, S. T.; *Thin Solid Films* **2020**, *711*, 138272. [Crossref]
59. Raman, S.; Arunagirinathan, R. S.; *Nanomaterials* **2022**, *12*, 1932. [Crossref]

Submitted: February 20, 2024
Published online: July 11, 2024